Article

Electrochemical Properties of Sputtered Ruthenium Oxide Neural Stimulation and Recording Electrodes

Bitan Chakraborty [1*]

[1] Department of Materials Science and Engineering, University of Texas at Dallas, Richardson, TX, 75080, USA; bitan.chakraborty@utdallas.edu
* Correspondence: bitan.chakraborty@utdallas.edu

Abstract: A chronically stable electrode material with low impedance for recording neural activity and high charge-injection capacity for functional electro-stimulation is desirable for the fabrication of implantable microelectrode arrays that aims to restore impaired or lost neurological functions in humans. For this purpose, we have investigated the electrochemical properties of sputtered ruthenium oxide (RuOx) electrode coatings, deposited on planar microelectrode arrays, using an inorganic model of interstitial fluid (model-ISF) at 37° C as the electrolyte. Through a combination of cyclic voltammetry (CV) and electrochemical impedance spectroscopy (EIS) modelling study we have established the contribution of faradaic reaction as the major charge-injection contributor within the safe neural stimulation potential window of ±0.6 V vs Ag|AgCl. We have also established the reversibility of the charge-injection process for sputtered RuOx film by applying constant charge-per-phase current stimulations at different pulse widths and by comparing the magnitudes of leading and trailing access voltages during voltage transient measurements. Finally, the impedance of the sputtered RuOx film was found to be reasonably comparable in both its oxidized and reduced states, although electronic contribution from capacitive double-layer was found to be slightly higher for the completely oxidized film around 0.6 V than its reduced counterpart around -0.6V.

Keywords: ruthenium oxide; charge-injection; impedance; neural stimulation; neural recording

1. Introduction

Electrode coatings are integral parts of implantable microelectrode arrays (MEAs), that are intended to restore lost or impaired physiological functionality in humans. Clinical applications, that use MEAs, include the use of brain-machine interfaces (BMIs) that allows volitional control of robotic assistive prosthetics, restoration of vision and sensory feedback for amputees [1-5]. Electrode coatings are deposited on exposed electrode sites of the MEAs during the fabrication process and when implanted into the patients allow bi-directional communication between the device and the nervous system. Low impedance electrodes allow for recording single-units with high signal-to-noise ratios (SNRs) [6] and high charge-injection capacity allows for electrical stimulations for functional response with high current levels, without exceeding harmful potential limits [6,7]. However, MEAs are known to decline in stimulation and recording performance overtime, due to a number of failure mechanisms thereby making it challenging to establish chronic neural interface [8].

Although noble metal electrodes are useful for recording neural activity, including resolving single action potentials (single units), the charge-injection levels for functional electrical stimulation are well beyond their capacity [9,10]. It is therefore necessary to investigate electrode materials with low-impedance that allow injection of appropriate levels of charge to evoke functional responses without undergoing corrosion or reaction with the tissue to produce toxic by-products at the electrode-tissue interface. Additionally,

 doi:10.20944/preprints202306.1053.v1

these high charge capacity electrodes must be stable in the physiological environment chronically.

Materials investigated as electrode coating in MEAs include platinum (Pt), platinum/iridium (Pt/Ir), titanium nitride (TiN), conducting polymers, like PEDOT:PSS and iridium oxide [10–13]. The performance of these electrode materials for neural stimulation has been detailed in several comprehensive reviews [6,7]. Here, we report on ruthenium oxide (RuOx) as a possible electrode coating candidate for neural stimulation and recording. Previously, we have reported on the microstructure, charge-storage and charge delivery properties of the sputtered RuOx films with respect to change in reactive gas ratios (O_2:H_2O) during DC magnetron sputtering [14,15]. The charge-injection characteristics, resistance to oxygen reduction and long-term pulsing stability in buffered saline solution for this sputtered RuOx film were also established in previous studies [15,16]. In this study, we have further investigated the electrochemical properties, particularly the charge delivery mechanism, contribution of different circuit components, reversibility of charge-injection and the impedance states during electrochemical stimulation of the RuOx film, sputtered using a previously identified optimal oxygen to water vapor ratio of 1:3, in the reactive plasma, using an inorganic model of interstitial fluid (model-ISF) at 37° C.

The RuOx film was sputter deposited on exposed gold sites of a planar microelectrode array resulting in circular electrodes of 50 µm diameter, which amounts to a geometric surface area of ~1960 µm^2. To understand the charge injection mechanism, the electrochemical properties of these planar electrodes were studied in model-ISF at 37° C using electrochemical techniques like cyclic voltammetry (CV), electrochemical impedance spectroscopy (EIS) and voltage transient measurements. Impedance modelling study was performed using Randles' circuit model [17] to understand the contributions of different circuit components during charge injection. The circuit components allow us to probe into the different contributors to the charge injection. We find that the faradaic component is the major contributor for electrochemical charge injection into model-ISF at 37° C. The capacitive component is also found to be a secondary contributor to the charge injection, therefore making the sputtered RuOx a mixed conductor [6]. The sputtered RuOx film conduction, associated with electronic contribution from capacitive double-layer, was found to be slightly higher for the oxidized state at 0.6 V in comparison to the reduced state at -0.6 V, although the impedance trend across these voltages at 1 Hz, 1 kHz and 100 kHz frequencies were found to be constant.

For continuous and chronic neural stimulation, it is important that reactions occurring during charge injection must be reversible. Irreversible reactions can cause damage to the electrode coating exposing the electrode sites which in turn might cause unwanted tissue damage during stimulation. Through analytical studies of the sputtered RuOx coating by voltage transient measurements we have established reversibility of the faradaic reaction that contributes towards the charge injection. In a previous study we have already established the capability of this electrode coating to undergo constant current stimulation for up to 1 billion cycles in model-ISF at 37° C [16]. Therefore, by using the best practice stimulation waveforms [6] we can safely inject charge into the tissue via the sputtered RuOx electrode thus enabling continuous and chronic functional neural stimulation.

2. Materials and Methods

2.1. Planar Microelectrode Fabrication

The planar microelectrode arrays were fabricated on 100 mm diameter single crystal silicon wafers following microfabrication procedure described previously [14,18]. Briefly, 2 µm amorphous silicon carbide (a-SiC) was deposited on the wafer by plasma enhanced chemical vapor deposition (PECVD). Using lift-off photolithography gold (Au) metal traces were sputter deposited using Ar plasma in an AJA ATC 2200 (AJA Internationals, Scituate MA) DC magnetron sputtering system. A second 2 µm a-SiC layer was deposited on top the Au layer, in effect making a 200 nm patterned Au trace sandwiched between 4 µm a-SiC. The bond pads and 50 µm diameter electrode sites were created using reactive

Preprints (www.preprints.org) | NOT PEER-REVIEWED | Posted: 14 June 2023 doi:10.20944/preprints202306.1053.v1

ion etching of the a-SiC using SF_6/O_2 plasma. Finally, using lift-off photolithography, sputtered ruthenium oxide film, using a 1:3 O_2:H_2O ratio in the reactive plasma, was deposited on the electrode sites. Details of the ruthenium oxide deposition process has been described previously [14]. Figure 1(a) shows an optical image of the circular fabricated electrode sites. Figure 1(b) shows a scanning electron microscopic (SEM) image of a single circular electrode site coated with sputtered RuOx film.

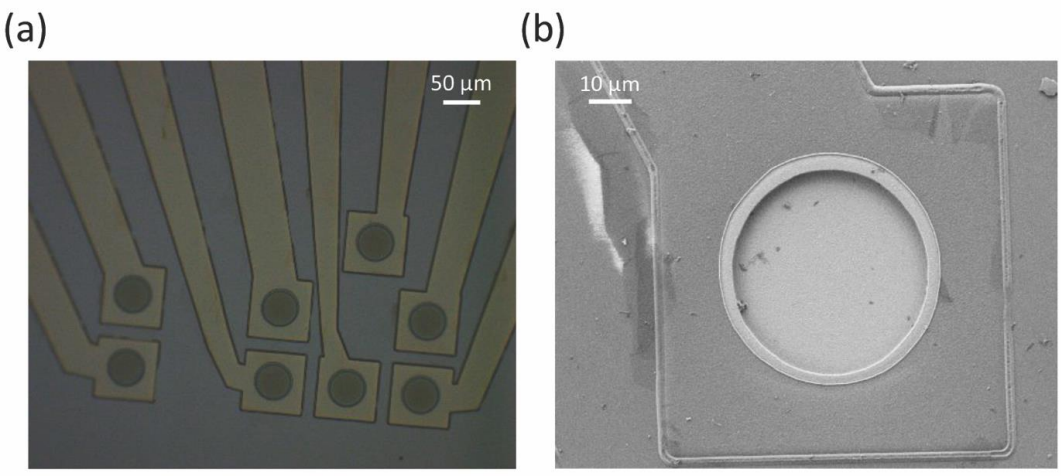

Figure 1. A fabricated planar microelectrode array with sputtered RuOx electrode sites of 50 µm diameter. (**a**) Image taken at 20x magnification in an optical microscope. (**b**) Image of an electrode site taken using a scanning electron microscope.

2.2. Electrolyte Preparation

All electrochemical measurements were performed in either phosphate buffered saline (PBS) at room temperature (~20° C) or in an inorganic model of the interstitial fluid (model-ISF) at 37° C, which resembles the physiological environment more closely than PBS [19]. The pH and the conductivity of these electrolytes were measured using a Thermo Scientific Orion pH-meter and a Fischer Scientific, Traceable Bench Conductivity Meter respectively. The PBS solution comprised 126 mM NaCl, 22 mM $NaH_2PO_4.7H_2O$ and 81 mM $Na_2HPO_4.H_2O$ with a pH of 7.2 and ionic conductivity of 25 mS cm^{-1}. The model-ISF comprised of 110 mM NaCl, 28 mM $NaHCO_3$, 7.5 mM $KHCO_3$, 2 mM $Na_2HPO_4.7H_2O$, and 0.5 mM each of $NaH_2PO_4.H_2O$, $MgSO_4$, $MgCl_2$, and $CaCl_2$. The pH was maintained at a near physiological level of 7.4 by purging mixed gas consisting of 5% CO_2, 6% O_2 and 89% N_2 for at least 30 minutes. Thereafter, the gas mixture was left to flow continuously over the surface of the solution during any electrochemical measurements. The ionic conductivity of model-ISF was 15 mS cm^{-1} and a laboratory oven was used to conduct measurements for this electrolyte in order to maintain a near physiological temperature of 37° C.

2.3. Cyclic Voltammetry

A three-electrode configuration consisting of a Ag|AgCl reference electrode, a large surface area Pt wire counter electrode and sputtered RuOx working electrode was used for all the electrochemical measurements. The cyclic voltammetry (CV) measurements were performed using a Gamry Reference 600+ potentiostat using vendor-provided data acquisition software. For CV measurement, the potential was modulated with triangular waveform at sweep rates of 50 mV s^{-1}. Potential limits of -0.9/0.9 V, -0.8/0.8 V, -0.7/0.7 V and -0.6/0.6 V vs Ag|AgCl were implemented to carry out the CVs to establish the water electrolysis window for safe stimulation.

2.4. Electrochemical Impedance Spectroscopy

Similar to the CVs, the electrochemical impedance spectroscopy (EIS) was also measured using three-electrode configuration with a Gamry Reference 600+ potentiostat. EIS

Preprints (www.preprints.org) | NOT PEER-REVIEWED | Posted: 14 June 2023 doi:10.20944/preprints202306.1053.v1

measurements were obtained using a 10 mV root-mean-square (rms) AC sinusoidal excitation voltage over a frequency range of 0.1 to 10^5 Hz. The EIS was measured about the open circuit potential (E_{oc}) and over an applied DC voltage bias range from -0.6 V to 0.6 V vs the Ag|AgCl reference electrode, at 0.1 V increments. A time delay of 30 minutes was allowed between each EIS measurement to let the RuOx electrode reach equilibrium open circuit potential. A similar experiment was described previously to understand the effect of potential on electrode conductivity for electrochemically deposited iridium oxide (EIROF) electrodes [20].

2.5. Voltage Transient Measurements

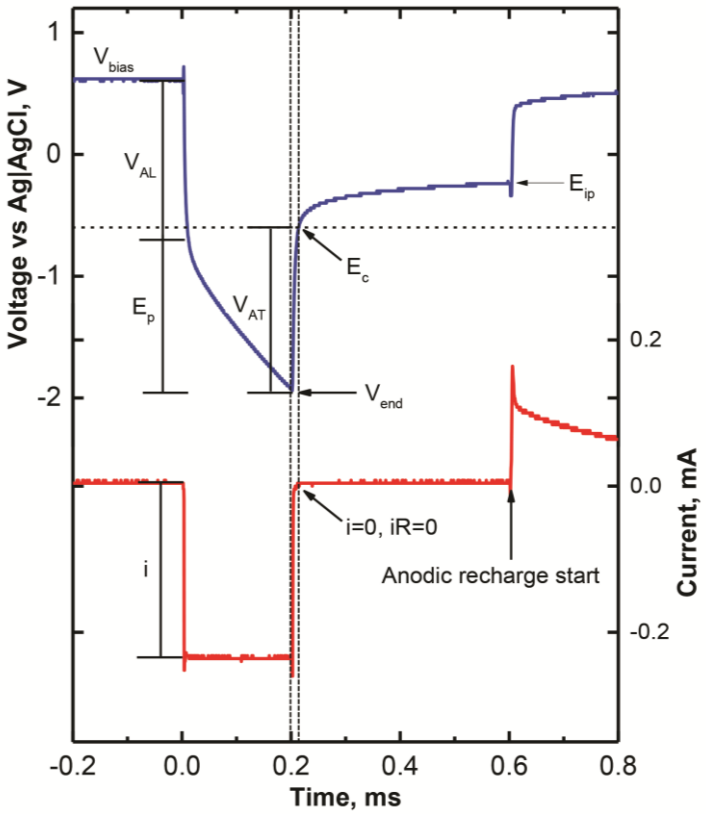

Figure 2. A representative voltage transient of a sputtered ruthenium oxide electrode in response to a rectangular cathodal current pulse.

Voltage transients in response to current pulsing were measured with a Sigenics stimulator (Sigenics, Chicago, IL) as described previously [18]. The stimulator uses a three-electrode configuration and providing rectangular cathodal current pulses, with adjustable pulse-width from 100 μs to 1000 μs. Charge-balance is achieved by actively controlling the interpulse potential of the electrode to a pre-determined interpulse bias level, usually 0.6 V vs. Ag|AgCl for ruthenium oxide and iridium oxide electrodes [14,18]. There is also an adjustable interphase period of 0.0-1.0 ms between the end of the cathodal current pulse and the beginning of the anodic recharge phase in which the electrode is electrically floating under open-circuit conditions with no applied current. The potential of the electrode in the zero-current interphase period is used as an estimate of the maximum negative electrode potential in response to current pulsing as overpotentials are minimized in the absence of an impressed current.

An example voltage transient in response to cathodal current pulsing of a RuOx electrode using ~250 μA, 200 μs pulses is shown in Figure 2. V_{AL} represents the access voltage at the leading edge of the current pulse and measured as the abrupt change in electrode voltage at the initiation of the current pulse. E_P represents the polarization across the electrode-electrolyte interface and together with V_{AL} defines the electrode driving voltage

Preprints (www.preprints.org) | NOT PEER-REVIEWED | Posted: 14 June 2023 doi:10.20944/preprints202306.1053.v1

($V_{drv} = V_{AL} + E_p$). V_{AT} represents the trailing phase of the access voltage and is calculated as the difference between the cathodal electrode potential (E_c) and the maximum negative voltage (V_{min}), which is observed at the end of the current pulse. E_c is measured in the interphase period, 12 µs after the end of the cathodal pulse when the current has decayed to zero (i=0, iR=0) so that the measured potential no longer includes a contribution from an ohmic voltage drop in the electrolyte. We define the maximum charge-injection capacity of the electrode to be that charge, at the pulsewidth at which the measurement is made, that polarizes the electrode to an E_c of -0.6 V vs. Ag|AgCl, This maximum potential excursion (E_{mc}) corresponds to a potential that is slightly positive of the water reduction potential on RuOx estimated from 50 mV s^{-1} CVs, and is the same E_{mc} typically employed in evaluating iridium oxide and platinum-based stimulation electrodes [6,9]. E_{ip} is the potential at the end of the zero-current interphase period just before the beginning of the anodic recharge current.

2.6. Statistical Analysis

Data sets were tested for normality using Shapiro-Wilk method with a level of significance $\alpha = 0.05$. All the normally distributed data sets, measured from electrodes of the same array, were reported as mean ± standard deviation (SD).

3. Results

3.1. Cyclic Voltammetry

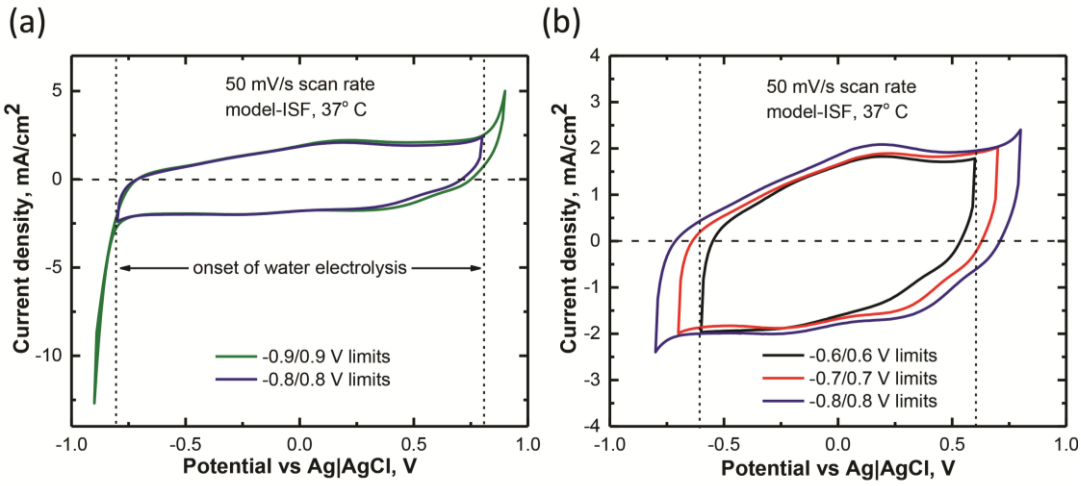

Figure 3. Cyclic voltammograms at a scan rate of 50 mV s^{-1} of sputtered RuOx electrodes in model-ISF at 37° C. (**a**) Comparison between CVs of the same electrode taken at scan range of -0.9 V to 0.9 V and -0.8 V to 0.8 V, showing the water electrolysis window from observation of high current onset.; (**b**) Comparison between CVs at three different scan range, of -0.8 V to 0.8 V, -0.7 V to 0.7 V and -0.6 V to 0.6 V.

In Figure 3a we observe a very high current-onset at both positive and negative ends of a cyclic voltammogram for a -0.9/0.9 V potential range vs Ag|AgCl compared to a -0.8/0.8 V potential range CV in model-ISF at 37° C. Such large current-onset associated with charge-injection electrodes is attributed to water electrolysis reaction, where water is reduced at the negative end and oxidized at the positive end [6]. Therefore, the potential limits for water electrolysis of RuOx were set based on the observed onset of large reduction and oxidation currents respectively at -0.8 V and 0.8 V in model-ISF at 37° C, as shown in Figure 3b. Although a -0.7 V to +0.7 V (Ag|AgCl) potential range (Figure 3b) seemed to be within the water electrolysis window, a potential range of -0.6 V to 0.6 V is chosen as potential limits for safe stimulation. Therefore, most of the analysis was based on CVs with -0.6 V to 0.6 V scan range.

Preprints (www.preprints.org) | NOT PEER-REVIEWED | Posted: 14 June 2023 doi:10.20944/preprints202306.1053.v1

3.2. Electrochemical Impedance Characteristics

The EIS in model-ISF at 37° C were measured as a function of DC bias voltages from 0.6 to -0.6 V vs Ag|AgCl with an increment of 0.1 V to understand the effect of potential on the conductivity of the sputtered ruthenium oxide electrodes. A time delay of 30 minutes was allotted between each EIS measurement to allow the RuOx electrode to reach equilibrium open circuit potential. Figure 4a shows the Bode plot for EIS measurements of RuOx electrodes (mean ± SD, n=3) as a function of bias. The impedance plots measured at all the applied bias values were found to be on top of each other along the entire frequency range. The impedance values at 1 Hz, 1 kHz and 100 kHz (mean ± SD, n=3) is also plotted in association with cyclic voltammogram on a common voltage axis (x-axis) in Figure 4b. A similar absence of bias dependence across this frequency range is also observed for sputtered iridium oxide but not for activated or electrodeposited iridium oxide [20,26–28]. The bias dependence of activated and electrodeposited iridium oxide has been attributed to the low density of these oxides combined with a notable decrease in electronic conductivity when the oxide is in the Ir^{3+} redox state [28]. Similarly, it appears that the density of sputtered RuOx is sufficient to maintain an adequately low impedance in the reduced films to support charge injection, as evidenced by the substantial cathodal currents observed in the CV response of RuOx at negative potentials.

No observable changes in these values were found associated with the change in potential for all three chosen frequency. Therefore, the sputtered ruthenium oxide film is almost equally impeding in both its oxidized and reduced states allowing reversibility during charge-injection.

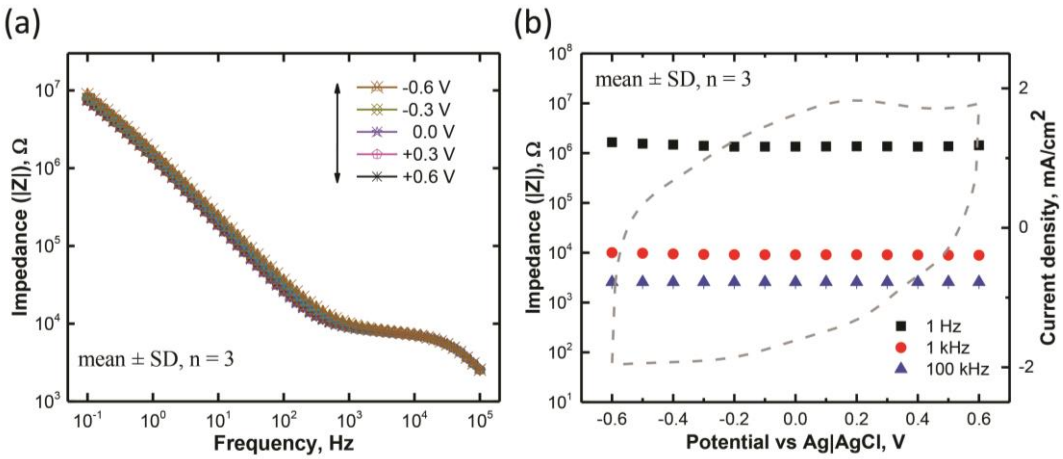

Figure 4. Impedance characteristics of sputtered RuOx electrode in model-ISF at 37° C. (**a**) Representative impedance curve for a sputtered RuOx electrode as a function of DC bias vs Ag|AgCl. (**b**) Impedance magnitude at 1, 10^3 and 10^5 Hz against DC bias plotted (x-axis) in comparison to CV plotted using same potential range (x-axis).

3.3. Impedance Modelling Study

A Randles' circuit model [17] was used to calculate the circuit elements from electrochemical impedance spectroscopy of sputtered RuOx electrodes. A similar model was used previously to characterize electrodes for biomedical implants that used sputtered iridium oxide films [21,22]. The model consists of contributions form electrolyte resistance (R_s), capacitive double-layer between the film and ions in the electrolyte (C_{dl}), resistance due to the Faradaic charge-transfer reaction in the ruthenium oxide (R_f) and a constant phase element (CPE), defined as by the CPE impedance as follows:

$$Z_{CPE} = \frac{1}{Y^o(j\omega)^a}, \quad (1)$$

where ω is the frequency, a is a number from 0-1 and Y^o is the coefficient of constant phase element with units S sa or sa Ω^{-1} cm^2 [23]. Gamry Echem Analyst software (Gamry

Preprints (www.preprints.org) | NOT PEER-REVIEWED | Posted: 14 June 2023 doi:10.20944/preprints202306.1053.v1

Instruments, Inc, PA) was used to for the impedance modelling analysis. The fit employed Nelder and Mead's simplex algorithm [24] allowing up to 300 iterations. The objective function (χ^2) was used to define the goodness of fit [25], such that a lower value of χ^2 implies a better fit. However, this model cannot account of fitting of high frequency and low frequency measurements, as previously predicted for iridium oxide electrodes [21].

We performed fitting on the EIS of sputtered RuOx films obtained in PBS as well as model-ISF at 37° C, over a frequency range of 0.1-10^5 Hz. The Bode plot for the measured EIS and the fitted results are shown in Figure 5a and b. The χ^2 values obtained were 0.0032 and 0.0078 respectively for PBS and model-ISF respectively. However, lowering the frequency range to 10-10^4 Hz, shows a better fit, as shown in the Bode plots in Figure 5c and d. The value obtained for this fit were 0.0008 for both PBS and model-ISF at 37° C and therefore a better goodness of fit was obtained for the 10-10^4 Hz frequency range. The circuit parameters are obtained for the sputtered RuOx electrodes in PBS and model-ISF from this frequency range and has been tabulated in Table 1.

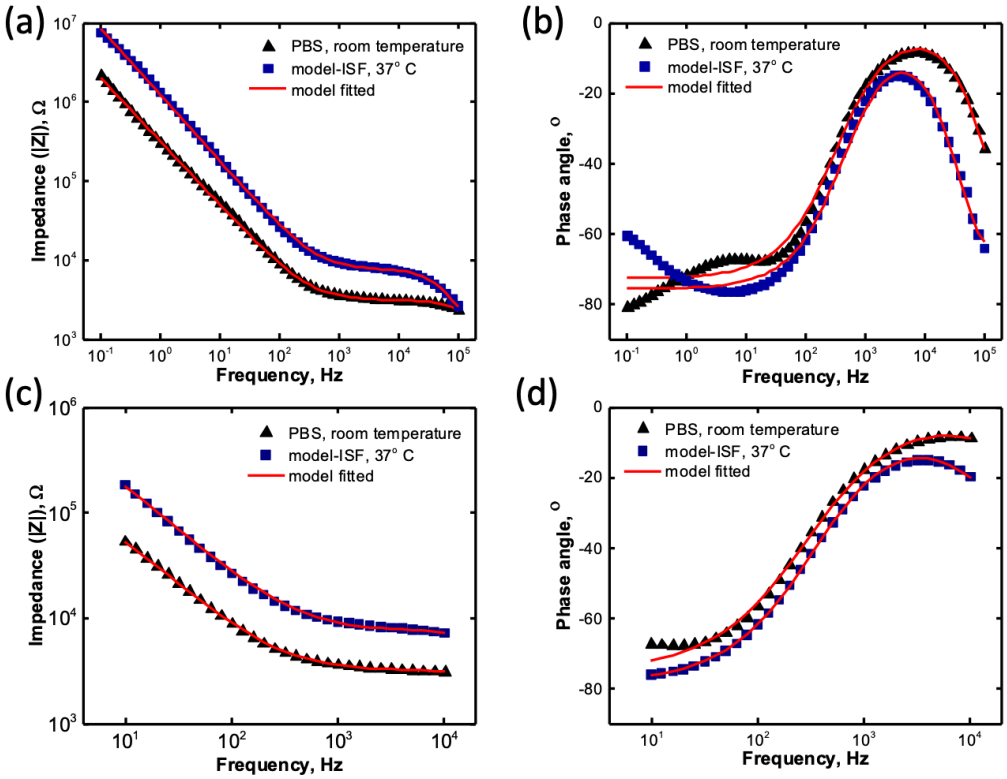

Figure 5. Bode plot for sputtered RuOx electrode fitted to Randles' circuit model. (**a**) The impedance plotted against the frequency range of 0.1-10^5 Hz. (**b**) The phase angle plotted against the frequency range of 0.1-10^5 Hz (**c**) The impedance plotted against the frequency range of 10-10^4 Hz (**d**) The phase angle plotted against the frequency range of 10-10^4 Hz.

Table 1. Circuit parameters evaluated from Randles' circuit model for sputtered RuOx electrode. Mean and standard deviation (SD) taken for n=3.

Electrolyte	R_s (kΩ) Mean ± SD	R_f (kΩ) Mean ± SD	C_{dl} (nF) Mean ± SD	Y^o (nS s^a) Mean ± SD	a Mean ± SD
PBS	2.32 ± 0.12	1.08 ± 0.14	6.54 ± 1.05	601.70 ± 30.90	0.85 ± 0.00
model-ISF	4.95 ± 0.62	2.96 ± 0.31	8.86 ± 3.75	328.90 ± 33.40	0.87 ± 0.01

3.4. Contribution of Circuit Componenets in Charge Injection

The EIS data obtained (Figure 4) by applying bias from -0.6 to 0.6 V is fitted using Randles' circuit (only within 10 to 10^4 Hz) and the percentage changes in circuit parameters from equilibrium value at open circuit potential is plotted in Figure 6. Figure 6 shows

Preprints (www.preprints.org) | NOT PEER-REVIEWED | Posted: 14 June 2023 doi:10.20944/preprints202306.1053.v1

the percentage charge in circuit components of EIS obtained at different bias levels vs Ag|AgCl with respect to EIS vs the open circuit potential, obtained by fitting the Randles' circuit model (shown in the inset of Figure 6) to the measured EIS in mISF at 37° C. About 5% increase in the component associated with double-layer capacitance, C_{dl} was obtained at 0.6 V potential. However, a decrease by ~5% of C_{dl} is observed at the -0.6 V potential. This is indicative of a higher electronic contribution towards double-layer capacitance associated with the completely oxidized state of the film at 0.6 V. In contrast the completely reduced film at -0.6 V has lower electronic conduction and therefore lower contribution towards C_{dl}.

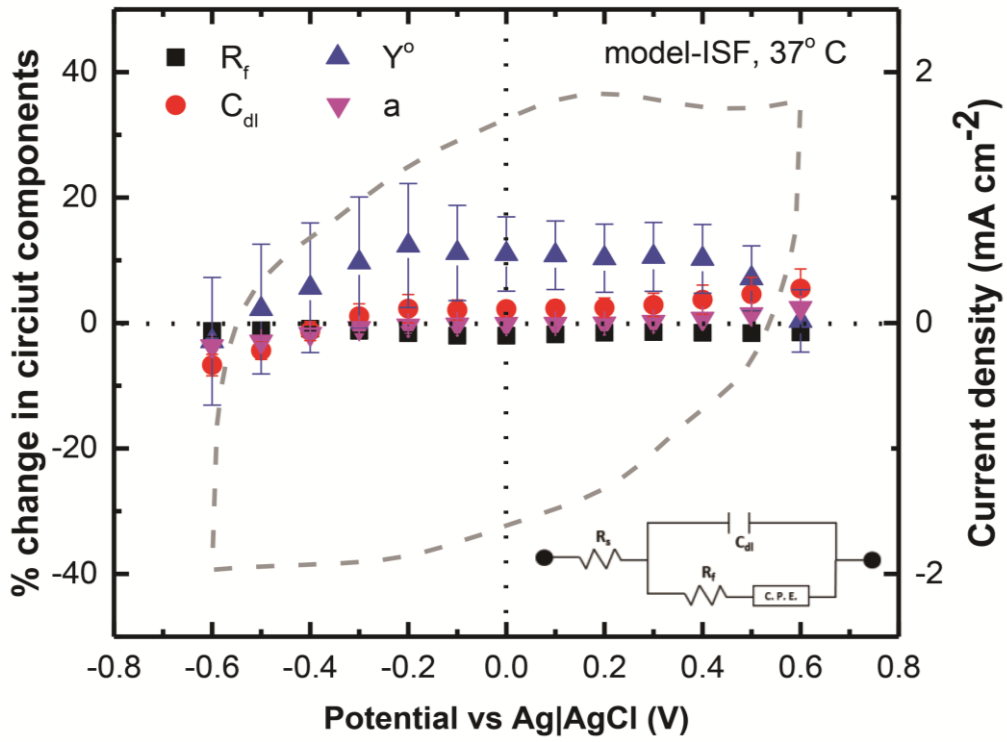

Figure 6. Percentage change in circuit components calculated from Randles' fit from measured EIS at different bias levels of -0.6-0.6 V vs Ag|AgCl with respect to circuit components modelled from EIS measured with respect to open circuit potential.

The constant phase coefficient, Y° shows an average (n=3) increase of ~10% for the potentials ranges of -0.4-0.4 V and falls off to the equilibrium value at both the positive and negative end of the CV. The initiation of increase in the Y° value was observed from 0.5 V at the oxidation end and the increased value was observed until -0.5 V at the reduction end. This is attributed to the initiation of the faradaic redox process at these potentials, also indicated by the redox peaks observed in the CV (plotted with the right y-axis on Figure 6). Between these potentials the film is in a redox transient state and therefore, the Y°, which is associated with redox reaction rates, have higher values, and also aligns with the redox peaks of the CV. The Y° value falls off to the equilibrium value indicating end point for the redox processes at both positive and negative end of the CV, where the film is in a completely oxidized state and completely reduced state respectively. We also observed that at 0 V vs the Ag|AgCl or at the open circuit potential value (vs Ag|AgCl) for RuOx film (~0.2 V) the percentage change in Y° value does not fall off to zero, which is expected. This is mostly likely because the time required to reach the equilibrium after biasing at higher potentials is more than 30 minutes used as delay for each EIS measurement. So, this observation is associated with a transient redox state of the film, rather than at its equilibrium state. Minimal changes in both R_f and "a" values of the circuit component were observed. The minimal change in R_f value, observed at all the bias levels

Preprints (www.preprints.org) | NOT PEER-REVIEWED | Posted: 14 June 2023 doi:10.20944/preprints202306.1053.v1

indicates a reversible redox process contributing to the charge-injection and that the ionic pathways are not impeded at these potential ranges (-0.6-0.6 V).

3.5. Charge Injection Reversibility

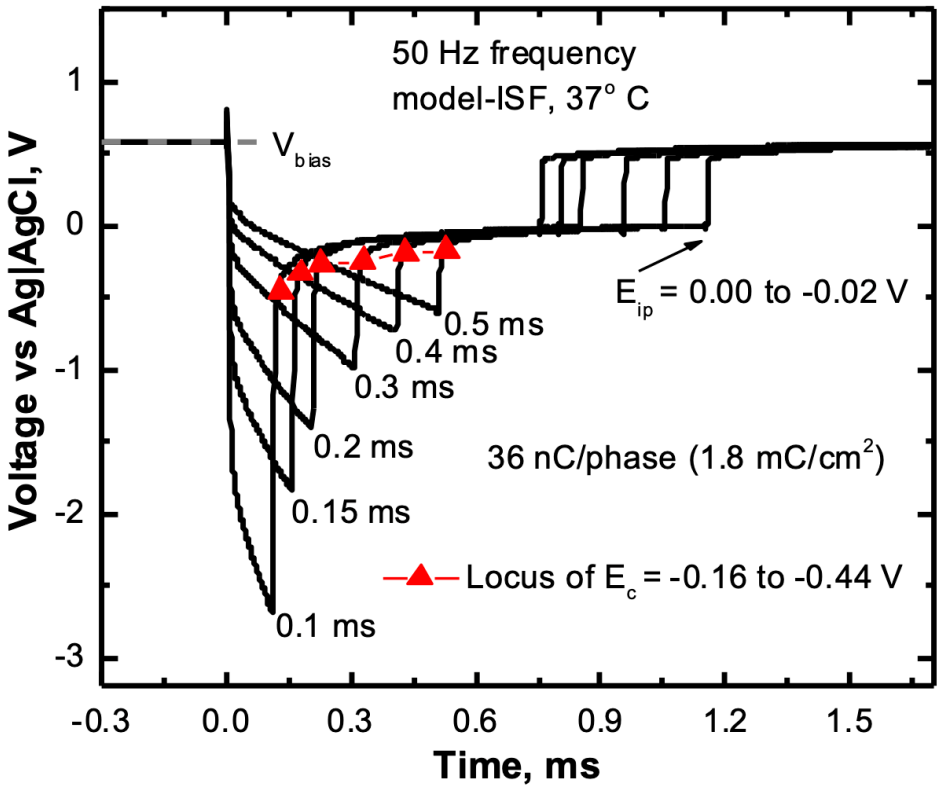

Figure 7. A comparison of voltage transient response of a sputtered ruthenium oxide microelectrode (GSA ~1960 μm2) at 36 nC phase^{-1} with pulse durations 0.1-0.5 ms.

The charge-injection capacity is dependent on current density and therefore to understand limitations of RuOx films during charge-injection we have measured the voltage transient at relevant current densities. Voltage transient response of a sputtered RuOx electrode at an interpulse bias of 0.6 V vs Ag|AgCl in response to a current pulse of 36 nC phase^{-1} or 1.8 mC cm^{-2} at six different pulse widths from 0.1 to 0.5 ms is plotted in Figure 7. The current waveform at 50 Hz consisted of cathodal current pulse followed by a zero-current interphase period of 0.7 ms before the anodic recharge phase sets in to reestablish the interpulse bias. To keep the charge per phase constant at 36 nC phase^{-1} we applied current densities from 3.67 A cm^{-2} to 18.34 A cm^{-2} for 0.5 ms to 0.1 ms cathodal pulse durations respectively. The E_c was found to vary from -0.16 V at 3.67 A cm^{-2} to -0.44 V at 18.34 A cm^{-2} corresponding to larger activation potential for higher current density. The E_{ip} values for the different pulse durations was also found to be very close to each other (~0.02 V) implying reversibility of the charge-injection process, especially at higher current densities. We also observe that the electrode potential during the zero-current interphase period recovers rapidly from E_c to E_{ip}, which indicates a fast equilibration of the reduced RuOx film during charge injection.

The voltage transient response as a function of current pulse amplitude using 0.6 V interpulse bias was examined to understand the change in film property during stimulation using a cathodal pulse at 0.2 ms pulse duration. Such voltage transients for a sputtered RuOx electrode are plotted in Figure 8a. The electrode cathodal potential (E_c) shifts negative, and the driving voltage (V_{drv}) increases with increasing current amplitude. We also observe minimum inflection in the polarization for all the current amplitudes. The magnitudes of the leading (V_{AL}) and trailing (V_{AT}) access voltages are also similar up to the point when the electrodes are polarized to an E_{mc} of – 0.6 V (Ag|AgCl). This effect is

Preprints (www.preprints.org) | NOT PEER-REVIEWED | Posted: 14 June 2023 doi:10.20944/preprints202306.1053.v1

further shown in detail in Figure 8b, where access voltages are plotted as a function of E_c with a representative CV from sputtered RuOx electrode (mean ± SD, n = 5) plotted on the same potential axis (0.6 V to – 0.6 V). The values of V_{AL} and V_{AT} were found to be very close to each other in going from 0.6 V to – 0.6 V, which is different from AIROF or EIROF electrodes and similar to SIROF [6,20]. The implication is that the admittance of sputtered RuOx film is comparable in both its oxidized and reduced state and is consistent with the previous assessment from the study of impedance by applying DC bias against the reference electrode.

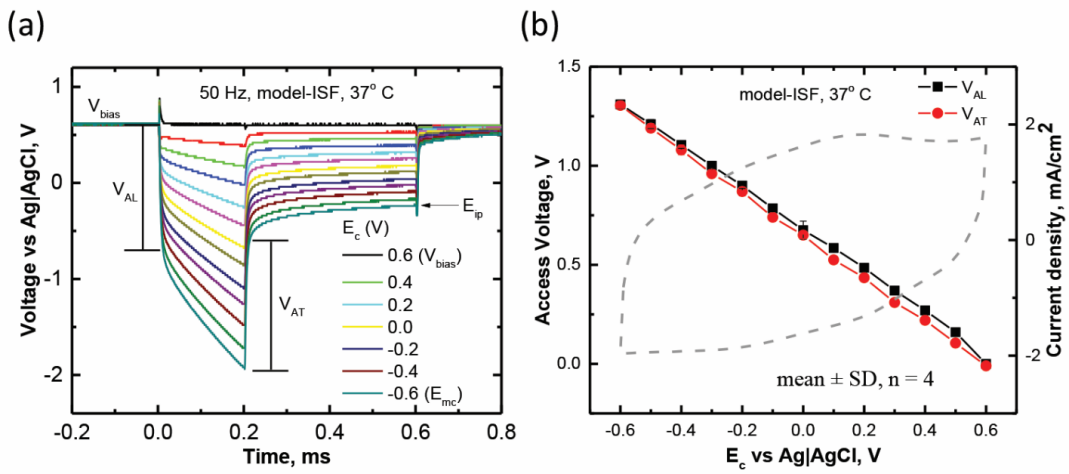

Figure 8. (**a**) Voltage transient response of a sputtered RuOx microelectrode as it is polarized to different potential excursions (E_c) starting from 0.6 V bias to an E_{mc} value of -0.6 V. (**b**) Comparison of V_{AL} and V_{AT} as a function of E_c (at 50 Hz, 0.6 V bias and 0.2 ms pulse duration). A CV curve is plotted on the right y-axis for comparison with the same potential range in the x-axis.

4. Discussion

We have investigated the electrochemical properties of sputtered RuOx electrode coatings relevant to their use as neural stimulation and recording electrodes. The study was conducted in model-ISF at 37° C as the electrolyte and with a -0.6/0.6 V potential window as the safe stimulation limits. The EIS study and analysis in Figure 4b at 3 different frequencies shows no change in |Z| values within the stimulation safe limits. This indicates that the sputtered ruthenium oxide film is almost equally impeding in both its oxidized and reduced states allowing reversibility during charge-injection. This observation is also consistent with the voltage transient measurement analysis study shown in Figure 8. No observable difference between the leading and trailing access voltages (V_{AL} and V_{AT} respectively) during charge injection stimulation with safe stimulation limits were found, as shown in Figure 8b. Therefore, it is clear that the impedance states of this electrode coating do not change between the safe charge injection potential limits. However, sputtered RuOx is a pseudo-capacitive electrode and therefore it is difficult to isolate the effect of only the Ru^{4+}/Ru^{3+} reversible faradaic charge-injection mechanism. So, we cannot state with certainty that the impedance of the oxide in Ru^{4+} and Ru^{3+} valence states are equal. For this reason, the EIS modeling study of the RuOx electrode coating was performed in terms of a suitable circuit model because it would shed some light on the impedance states of the two oxidation states of Ru as well as the charge-injection mechanism.

The Randles' circuit EIS modelling on the sputtered RuOx coatings and the analysis of the different circuit elements within the safe limits of electrochemical charge injection gives us a preliminary understanding of the charge-injection mechanism. From Figure 6, we observe that the faradaic impedance (R_f) does not change, and the coefficient of constant phase element (Y^o) has increased value with the -0.5/0.5 V window. The Y^o being inversely related to Z_{CPE} is indicative of the admittance state of the RuOx film contributed from only the faradaic charge transfer. Therefore, it is clear that the major contributor for

 doi:10.20944/preprints202306.1053.v1

the charge injection is the faradaic contribution or the ionic contribution where Ru^{4+}/Ru^{3+} transition occurs with the participation of a counter-ion from the electrolyte. Additionally, we observe that there is a positive percentage change of the C_{dl} component within -0.3 to 0.6 V, which is indicative of a higher electronic contribution towards double-layer capacitance associated with the oxidized state of the film, which is the Ru^{4+}, as indicative from a previous XPS analysis [14]. Further, a ~5% increase in C_{dl} at 0.6 V and a ~5% decrease in C_{dl} at -0.6 V with respect to the equilibrium state indicates a higher electronic conduction towards double-layer capacitance associated with the completely oxidized state of the film (Ru^{4+}) at 0.6 V in contrast to the lower electronic conduction of the completely reduced state of the film (Ru^{3+}) at -0.6 V. However, it is clear from this study that the sputtered RuOx is a mixed conductor, where contribution from electrons and ions partake in the charge-transfer mechanism. This is consistent with previous studies [29] and is also similar to an iridium oxide film that are currently used for neural stimulation and recording [6].

We have also studied the reversibility of the charge injection mechanism for the sputtered RuOx film. To perform safe neural stimulation as well as record neural single units with good SNR chronically and consistently, reversibility of the film state after an applied charge injection waveform is crucial. Our study indicates that during stimulation the electrode potential during the zero-current interphase period recovers rapidly from E_c to E_{ip} (Figure 7), indicating a fast equilibration of the reduced RuOx film during charge injection. This observation is similar to that in an activated iridium oxide film (AIROF), reported previously [6] and is attributed to the rapid internal equilibration of the non-uniformly reduced RuOx film to reach a uniform potential (E_{ip}) throughout the film. This non-uniform reduction is due to non-uniform current distribution, leading to larger potential at the edges of electrodes, which is a known limitation of voltage transient measurements [6]. There is also non-uniform potential distribution though the thickness of porous three-dimensional structure of RuOx, which is very similar to a sputtered or activated iridium oxide films [6,14,18]. Additionally, diffusion-controlled dissipation of the counter-ion concentration gradient within the porous film and the adjacent electrolyte reestablishes the counter-ions concentrations levels to that of the pre-pulse condition. An associated change in the electrode potentials occurs. This also contributes to the rapid potential shift in the interphase period [6].

From previous studies of the sputtered RuOx film we found that the counter ion contribution comes from the H^+ ion in the electrolyte [14,15]. Consistent with our results and analysis we propose a charge injection model associated with the sputtered RuOx film, as shown in Figure 9, consistent with a previous model studied from iridium oxide films [6]. Charge is injected into tissue from valence changes in multivalent (+4/+3) RuOx electrode coating that undergo reversible reduction-oxidation (redox) reactions [6]. The equation (2) shows the reversible redox reaction associated with the ionic contribution indicated in this charge injection model.

$$RuO_x(OH)_y + \delta H^+ + \delta e^- \leftrightarrow RuO_{n-\delta}(OH)_{n+\delta} \quad (2)$$

The sputtered RuOx is therefore a mixed conductor, exhibiting both electron and ion transport within the bulk of the coating, similar to an iridium oxide film [6]. The three-dimensional structure of the coatings provides more charge for stimulation, but access to this charge is limited by the rate of electron and ion transport within the coating [6].

The study of the electrochemical charge injection mechanism of the sputtered ruthenium oxide electrode coating indicates that this film can deliver charge reversibly into the tissue and is capable of chronic neural stimulation and recording. Although this study is consistent with the previous literature and corroborates well within the scope of our experiments and analysis, we would like to point out that our model is a simplistic one and must not be extended to animal models, where electrolyte inhomogeneity exists. An in-depth electrochemical modelling study of these and similar electrode coatings is currently underway. Additionally, chronic *in vivo* study using these electrode coating is also

Preprints (www.preprints.org) | NOT PEER-REVIEWED | Posted: 14 June 2023 doi:10.20944/preprints202306.1053.v1

currently underway and will pave the path for the use of these electrode coatings in FDA approved neural implants.

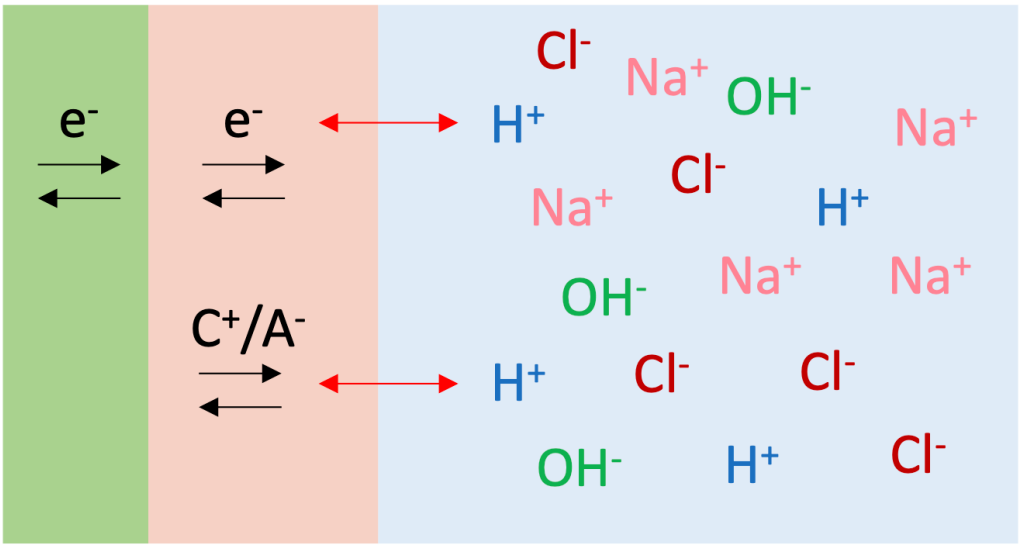

Figure 9. The three-dimensional faradaic charge injection mechanism of sputtered RuOx electrode. C^+ indicates cation and A^- indicates anion.

5. Conclusions

The electrochemical properties of the sputtered ruthenium oxide film as an electrode coating for neural stimulation and recording is presented in this work. The sputtered RuOx film was found to be almost equally impeding in its oxidized and reduced state at 0.6 V and -0.6 V respectively, indicating the ease of stimulation by either cathodal or anodal currents for monophasic current stimulation protocols. The oxidized film has comparatively higher contribution from double-layer capacitance than its reduced state. The faradaic redox process is dominant in the -0.5-0.5 V potential range vs Ag|AgCl, primarily contributing towards charge-injection. The fast reversibility in oxidation states of the sputtered RuOx film during stimulation ensures no irreversible side reactions during stimulation. The reversible charge injection mechanism allows for safe neural stimulation without producing any toxic side products and tissue damage as well as chronic neural recording capability. Previously, we have also established that this film does not contain extractable cytotoxic constituents and was, therefore, deemed non-cytotoxic in accordance to ISO protocol 10993-5 [30]. Additionally, RuOx films sputtered from ruthenium targets are cost-effective alternative to SIROFs, sputtered from iridium targets, which costs more than 10 times than that of ruthenium.

Author Contributions: Not applicable.

Funding: This research was funded by the grant NIH 5R01NS104344-02

Institutional Review Board Statement: Not applicable.

Informed Consent Statement: Not applicable.

Data Availability Statement: Not applicable.

Acknowledgments: The author would like to express sincere thanks to Dr. Stuart F. Cogan, Professor of Bioengineering at the University of Texas at Dallas for providing funding, resources, and valuable input for this work. The author would also like to thank Dr. Alexandra Joshi-Imre, Process Engineer at the Cleanroom Research Laboratory at the University of Texas at Dallas for helping with the SEM image. The author would like to acknowledge the University of Texas at Dallas Natural Sciences and Engineering Research Laboratory cleanroom staffs for their support in maintenance of all the equipment for device fabrication.

Conflicts of Interest: The author declares no conflict of interest.

References

1. Flesher, S.N.; Collinger, J.L.; Foldes, S.T.; Weiss, J.M.; Downey, J.E.; Tyler-Kabara, E.C.; Bensmaia, S.J.; Schwartz, A.B., Boninger; M.L.; Gaunt, R.A. Intracortical microstimulation of human somatosensory cortex. *Science translational medicine* **2016**, *8(361)*, pp.361ra141-361ra141.
2. Dhillon, G.S. and Horch, K.W. Direct neural sensory feedback and control of a prosthetic arm. *IEEE transactions on neural systems and rehabilitation engineering* **2005**, *13(4)*, pp.468-472.
3. Tomlinson, T.; Miller, L.E. Toward a proprioceptive neural interface that mimics natural cortical activity. *Progress in Motor Control: Theories and Translations* **2016**, pp.367-388.
4. Humayun, M.S.; Weiland, J.D.; Fujii, G.Y.; Greenberg, R.; Williamson, R.; Little, J.; Mech, B.; Cimmarusti, V.; Van Boemel, G.; Dagnelie, G.; de Juan Jr, E. Visual perception in a blind subject with a chronic microelectronic retinal prosthesis. *Vision research* **2003**, *43(24)*, pp.2573-2581.
5. Bradley, D.C.; Troyk, P.R.; Berg, J.A.; Bak, M.; Cogan, S.; Erickson, R.; Kufta C.; Mascaro, M.; McCreery, D.; Schmidt, E.M.; Towle, V.L. Visuotopic mapping through a multichannel stimulating implant in primate V1. *Journal of neurophysiology* **2005**, *93(3)*, pp.1659-1670.
6. Cogan, S.F. Neural stimulation and recording electrodes. *Annu. Rev. Biomed. Eng.* **2008**, 10, pp.275-309.
7. Merrill, D.R., Bikson, M. and Jefferys, J.G. Electrical stimulation of excitable tissue: design of efficacious and safe protocols. *Journal of neuroscience methods* **2005**, *141(2)*, pp.171-198.
8. Barrese, J.C.; Rao, N.; Paroo, K.; Triebwasser, C.; Vargas-Irwin, C.; Franquemont, L.; Donoghue, J.P. Failure mode analysis of silicon-based intracortical microelectrode arrays in non-human primates. *Journal of neural engineering* **2013**, *10(6)*, p.066014.
9. Negi, S.; Bhandari, R.; Rieth, L.; Solzbacher, F. In vitro comparison of sputtered iridium oxide and platinum-coated neural implantable microelectrode arrays. *Biomedical materials* **2010**, *5(1)*, p.015007.
10. Rose, T.L.; Robblee, L.S. Electrical stimulation with Pt electrodes. VIII. Electrochemically safe charge injection limits with 0.2 ms pulses (neuronal application). *IEEE Transactions on Biomedical Engineering* **1990**, *37(11)*, pp.1118-1120.
11. Weiland, J.D.; Anderson, D.J.; Humayun, M.S. In vitro electrical properties for iridium oxide versus titanium nitride stimulating electrodes. *IEEE transactions on biomedical engineering* **2002**, *49(12)*, pp.1574-1579.
12. Beebe, X.; Rose, T.L. Charge injection limits of activated iridium oxide electrodes with 0.2 ms pulses in bicarbonate buffered saline (neurological stimulation application). *IEEE transactions on biomedical engineering* **1988**, *35(6)*, pp.494-495.
13. Du, Z.J.; Luo, X.; Weaver, C.L.; Cui, X.T. Poly (3, 4-ethylenedioxythiophene)-ionic liquid coating improves neural recording and stimulation functionality of MEAs. *Journal of Materials Chemistry C* **2015**, *3(25)*, pp.6515-6524.
14. Chakraborty, B.; Joshi-Imre, A.; Maeng, J.; Cogan, S.F. Sputtered ruthenium oxide coatings for neural stimulation and recording electrodes. *Journal of Biomedical Materials Research Part B: Applied Biomaterials* **2021**, *109(5)*, pp.643-653.
15. Chakraborty, B.; Joshi-Imre, A.; Cogan, S.F. Charge injection characteristics of sputtered ruthenium oxide electrodes for neural stimulation and recording. *Journal of Biomedical Materials Research Part B: Applied Biomaterials* **2022**, *110(1)*, pp.229-238.
16. Chakraborty, B.; Joshi-Imre, A.; Cogan, S.F. Sputtered Ruthenium Oxide Neural Stimulation Electrodes. *43rd Annual International Conference of the IEEE Engineering in Medicine & Biology Society (EMBC)* **2021, November**, (pp. 6655-6658).
17. Randles, J.E.B. Kinetics of rapid electrode reactions. *Discussions of the faraday society* **1947**, *1*, pp.11-19.
18. Maeng, J.; Chakraborty, B.; Geramifard, N.; Kang, T.; Rihani, R.T.; Joshi-Imre, A.; Cogan, S.F. High-charge-capacity sputtered iridium oxide neural stimulation electrodes deposited using water vapor as a reactive plasma constituent. *Journal of Biomedical Materials Research Part B: Applied Biomaterials* **2020**, *108(3)*, pp.880-891.
19. Cogan, S.F.; Troyk, P.R.; Ehrlich, J.; Gasbarro, C.M.; Plante, T.D. The influence of electrolyte composition on the in vitro charge-injection limits of activated iridium oxide (AIROF) stimulation electrodes. *Journal of neural engineering* **2007**, *4(2)*, p.79.
20. Deku, F.; Joshi-Imre; A.; Mertiri, A.; Gardner, T.J.; Cogan, S.F. Electrodeposited iridium oxide on carbon fiber ultramicroelectrodes for neural recording and stimulation. *Journal of The Electrochemical Society* **2018**, *165(9)*, p.D375.
21. Weiland, J.D.; Anderson, D.J. Chronic neural stimulation with thin-film, iridium oxide electrodes. *IEEE Transactions on Biomedical Engineering* **2000**, 47(7), pp.911-918.
22. Franks, W.; Schenker, I.; Schmutz, P.; Hierlemann, A. Impedance characterization and modeling of electrodes for biomedical applications. *IEEE Transactions on Biomedical Engineering* **2005**, *52(7)*, pp.1295-1302.
23. Brug, G.J.; van den Eeden, A.L.; Sluyters-Rehbach, M.; Sluyters, J.H. The analysis of electrode impedances complicated by the presence of a constant phase element. *Journal of electroanalytical chemistry and interfacial electrochemistry* **1984**, *176(1-2)*, pp.275-295.
24. Dellis, J.L.; Carpentier, J.L. Nelder and Mead algorithm in impedance spectra fitting. *Solid state ionics* **1993**, *62(1-2)*, pp.119-123.
25. Sunde, S.; Lervik, I.A.; Tsypkin, M.; Owe, L.E. Impedance analysis of nanostructured iridium oxide electrocatalysts. *Electrochimica Acta* **2010**, *55(26)*, pp.7751-7760.
26. Fontes, M.B.A. Electrodes for bio-application: recording and stimulation. *Journal of Physics: Conference Series* **2013 March**, *Vol. 421, No. 1*, p. 012019.
27. Frederick, R.A.; Meliane, I.Y.; Joshi-Imre, A.; Troyk, P.R.; Cogan, S.F. Activated iridium oxide film (AIROF) electrodes for neural tissue stimulation. *Journal of Neural Engineering* **2020**, *17(5)*, p.056001.

 doi:10.20944/preprints202306.1053.v1

28. Pauporté, T.; Durand, R. Impedance spectroscopy study of electrochromism in sputtered iridium oxide films. *Journal of applied electrochemistry* **2000**, *30(1)*, pp.35-41.
29. McKeown, D.A.; Hagans, P.L.; Carette, L.P.; Russell, A.E., Swider, K.E.; Rolison, D.R. Structure of hydrous ruthenium oxides: implications for charge storage. *The Journal of Physical Chemistry B* **1999**, *103(23)*, pp.4825-4832.
30. Atmaramani, R.; Chakraborty, B.; Rihani, R.T.; Usoro, J.; Hammack, A.; Abbott, J.; Nnoromele, P.; Black, B.J.; Pancrazio, J.J.; Cogan, S.F. Ruthenium oxide based microelectrode arrays for in vitro and in vivo neural recording and stimulation. *Acta biomaterialia* **2020**, *101*, pp.565-574.